International Soil and Water Conservation Research 10 (2022) 240–253

Contents lists available at ScienceDirect

International Soil and Water Conservation Research

journal homepage: www.elsevier.com/locate/iswcr

Original Research Article

Multi-temporal modeling of road-induced overland flow alterations in a terraced landscape characterized by shallow landslides

Luca Mauri*, Eugenio Straffelini, Paolo Tarolli

Department of Land, Environment, Agriculture and Forestry, University of Padova, Agripolis, Viale Dell'Università 16, 35020, Legnaro (PD), Italy

ARTICLE INFO

Article history:
Received 9 February 2021
Received in revised form
6 May 2021
Accepted 7 July 2021
Available online 13 July 2021

Keywords:
Terraced landscape
Road
Landslide
Remote sensing
DEM

ABSTRACT

The presence of roads in high steep agricultural systems is often linked with landslides occurrence. This research aims to model multi-temporal overland flow dynamics in a shallow landslides-prone terraced landscape (northern Italy).The combined use of Remotely Piloted Aircraft Systems (RPAS) and photogrammetric techniques (e.g., Structure from Motion-SfM) allowed to elaborate multi-temporal high-resolution Digital Elevation Models (DEMs). Hydrological analyses of water flow's depth alterations due to the road presence were carried out adopting the SIMulated Water Erosion model (SIMWE), focusing on different scenarios considering the presence of the road and assuming its absence through a specific DEM smoothing procedure. The possibility to perform multi-temporal hydrological simulations at a hillslope scale so as to analyse the role played by the road in overland flows alteration is still a challenge to be investigated. Results proved the role played by the road in water flows change above the two observed shallow landslides, with respective maximum water depth values equal to 0.18 m and 0.14 m. On the contrary, no-road simulations not revealed significant water flows deviations towards landslides, with water depth values around 0 m, underlining that the absence of the road would avoid relevant changes in water flow paths toward the collapsed surfaces. This work could be a solid starting point for analyse road impact on runoff dynamics and hillslopes stability also at a wider scale, as well as for planning efficient mitigation intervention so as to reduce the occurrence of similar future scenarios.

1. Introduction

Nowadays, one of the major issues affecting agricultural systems is represented by the occurrence of land degradation processes (Bajocco et al., 2012; Romm, 2011; Tarolli & Straffelini, 2020), among which landslides and soil erosion by water are the most relevant ones (Tarolli et al., 2021). Land degradation in agriculture is due to several factors, such as changes in land use (Fagnano et al., 2012), land abandonment (López-Vicente et al., 2017; Louwagie et al., 2011), climate change (Webb et al., 2017), wildlife (Mauri et al., 2019) and increasing anthropogenic pressure (Sidle et al., 2014).

In this context, the presence of rural roads and the occurrence of land degradation processes, such as shallow landslides, are strongly connected (Eker & Aydin, 2014; Mauri et al., 2021; Wemple et al., 2001).

Road networks have numerous functions in agriculture, e.g., encourage efficient communications (Gollin & Rogerson, 2010), improve farmland management, and simplify farming operations (Sidle & Ziegler, 2012). On the other hand, despite their advantages, roads within a cultivated area can lead to the activation of slope failures. Several factors are involved in these processes. First, inefficient planning and design are responsible for activating landslides close to specific road sections (Marion & Leung, 2004; Salesa et al., 2019). Moreover, road construction induces failures on the undercut slope by altering of natural drainage systems (Sidle et al., 2006). Especially in steep slopes, banks stability can be seriously compromised due to the construction of a road (Sidle et al., 2006, 2014). The activation of landslides on steep slopes is also driven by the road-induced deviation and accumulation of the water, which successively infiltrates into soil layers above the potential slide plane (Keefer et al., 1987). Thus depends on several factors, e.g., pore-water pressure, drainage rate, antecedent precipitations, prior

* Corresponding author.
E-mail address: luca.mauri.2@phd.unipd.it (L. Mauri).

https://doi.org/10.1016/j.iswcr.2021.07.004

moisture content, slope materials, and road characteristics (Wieczorek, 1996; Guzzetti et al., 2007). Water infiltration and its subsurface accumulation increase the negative pore-water pressure (i.e., water pressure in unsaturated soil above the water table; Davison et al., 2000). The alteration of negative pore-water pressure is responsible for the progressive decrease of the unsaturated shear strength in the upper soil layers and consequently for landslides occurrence. In this regard, slope inclination and soil friction angle are also involved in failure dynamics. If on the one hand the reduction of stability of steep slopes is mainly driven by infiltration and consequent suction processes, on the other hand, the increase of negative pore-water pressure is mostly responsible for failures progressively affecting soft slopes (Gallage et al., 2021; Harp et al., 1990). Therefore, the drainage rate (i.e., the depth of water drained off from a specific area in a given time range) increases as the rainfall accumulates until the slope failure (Pamar, 2014).

Since water and road presence have a primary role in landslides occurrence, especially in steep slopes, temporal monitoring of roads-induced water direction alterations through the application of specific hydrological topographically-based models could help in understanding and, therefore, better managing the investigated issue. Digital photogrammetry (e.g., Structure from Motion- SfM) combined with Remotely Piloted Aircraft Systems (RPAS) allows realizing rapid and efficient analysis of surface topography through high-resolution Digital Elevation Models (DEMs) (Westoby et al., 2012). Therefore, the adoption of these technologies, combined with the use of hydrological models, represents an opportunity for the investigation of the relationship between road presence and landslides activation.

In light of the above considerations, this research proposes a multi-temporal hydrological analysis of the road role in the alteration of water flows in a shallow landslide-prone terraced agricultural system. SIMulated Water Erosion model (SIMWE; Mitasova et al., 2013) was adopted for the multi-temporal investigation of road influence on overland flow dynamics using RPAS-derived high-resolution DEMs. The application of such a model in the multi-temporal investigation of the interaction between road network, water overland flows deviation, and shallow landslides activation in the high-steep terraced vineyard is, in our knowledge, novel. The proposed research fills the gap in the scientific knowledge regarding the possibility to deeply analyse the presented environmental issue through the adoption of 4D RPAS-based digital terrain modeling, focusing on the evolution of hydrological processes over time at hillslope scale, and concurrently adopting a low cost and efficient methodology.

2. Study area

The study area is located in the Trento province, south of the Trentino Alto Adige region, northern Italy (Fig. 1a). It has an overall spatial extension equal to 2.2 ha, southwest aspect and an average slope of 27.6°, with an elevation between 266 m a.s.l. at the base and 320 m a.s.l. on the top (average value equal to 287 m a.s.l.). The annual average rainfall is 1088 mm, while inter-annual rainfall standard deviation is 222 mm. The study area is characterized by terraces built on steep slopes using earth banks, with an inter-row grass cover. Within the vineyard is located a road network, made to reach the highest terraces during agricultural operations. The

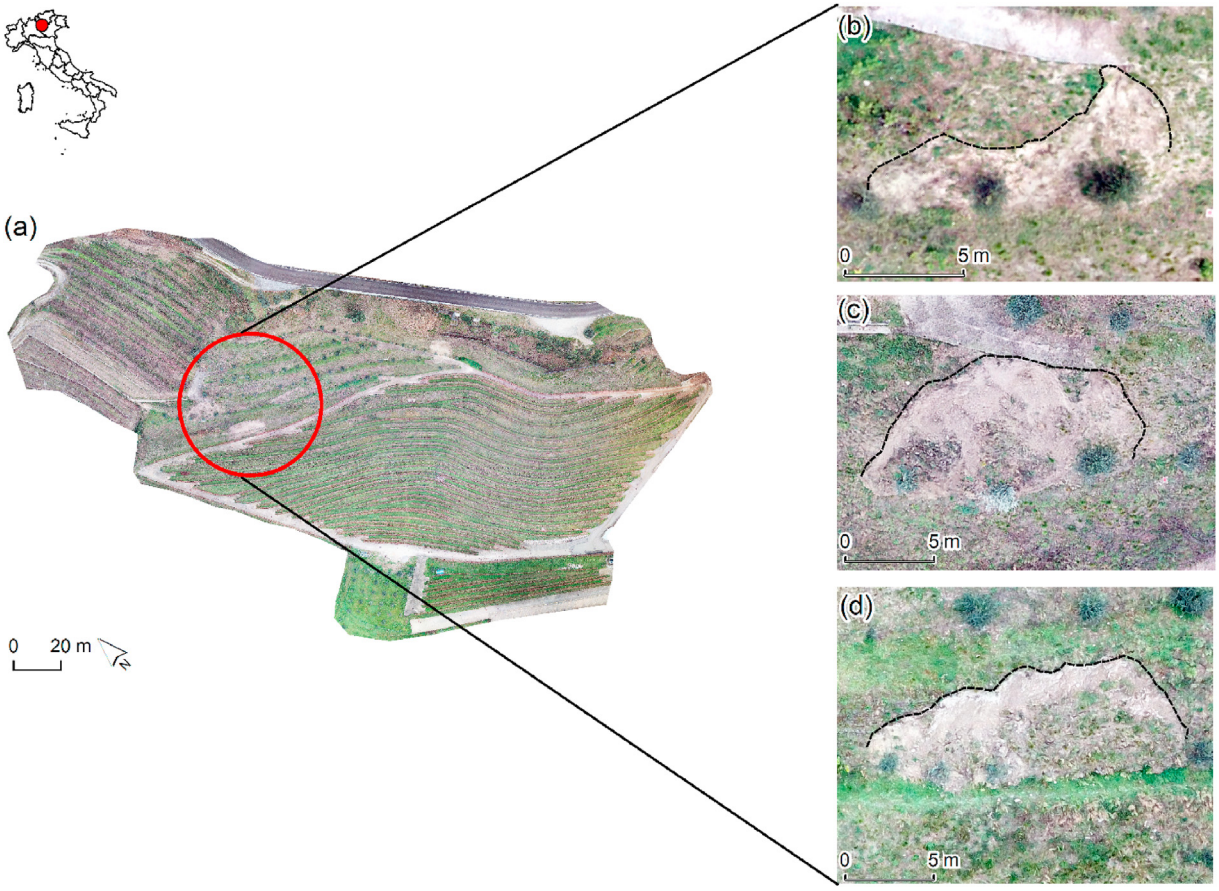

Fig. 1. Overview of the study area (a) and focus on the landslides L1-pre (b), L1-post (c) and L2 (d) observed during each RPAS survey. The pictures in Fig. 1b–d were manually taken through the RPAS surveys.

surface of the road is partly concrete, with some unpaved sections located around the whole vineyard. The road has a total length of about 600 m, with an average width of about 2 m, average slope equal to 15.7° (slope range between a minimum of 0.03° and a maximum of 19.2°). No drainage systems are located along the road, especially close to the landslide-prone banks, except for some paved sections located outside the rows where manholes are present.

During field surveys, two shallow landslides were observed. The first RPAS survey (18 October 2019) revealed the presence of a first landslide (L1-pre) below a paved section of the road (Fig. 1b). The second RPAS survey (17 December 2019) highlighted an evolution of L1 (therefore called L1-post) and the activation of a second shallow landslide (L2) about 20 m away from L1 and located close to an unpaved road section placed in the terraces above (Fig. 1c).

3. Material and methods

3.1. SIMulated Water Erosion (SIMWE) model

The plot-scale Simulated Water Erosion Model (SIMWE, Mitasova et al., 2013) is of great utility in the investigation of water and sediment dynamics at the hillslope scale. SIMWE is a bivariate physics-based and spatially distributed model able to simulate hydrologic overland water flows and sediment transport, with the possibility to estimate soil erosion starting from a single rainfall value. It implements a path sampling method by analysing superficial water flows processes and sediment transport separately, firstly modeling the superficial hydraulic flow tie-rod map and then using the obtained output for the calculation of the sediment runoff (Cencetti et al., 2005; Koco, 2011).

SIMWE is based on the principles describing the Water Erosion Prediction Project model (Flanagan & Nearing, 1995) and it is divided into two different components available in GRASS GIS environment, i.e., (i) r.sim.water and (ii) r.sim.sediment. Since the purpose of our work is to mainly focus on road-induced water dynamics alterations as a possible cause of landslides activation, the r.sim.sediment module was not considered in the analysis conducted in this work. The water module simulates overland water flows adopting a Green's function Monte Carlo path sampling method (Mitasova et al., 2004) whereby a system of differential equations is obtained by combining the mass conservation equation and the Manning relation (Cencetti et al., 2005). The continuity equation is solved assuming that water flow velocity depends on surface roughness and terrain slope and that it negligibly changes at a given location during the simulated event. Even though SIMWE does not consider antecedent moisture conditions for simulations, this model represents an optimal tool for the investigation of the issue presented in this work, starting from local rainfall peak and Manning's n inputs, to focus the analysis on road-overland flow-landslides interaction at hillslope scale among time.

SIMWE requires specific inputs for its modules. As far as the *r.sim.water* module is concerned, the necessary input data are (i) DEM (m), (ii) first-order x and y derivates of the DEM (−), (iii) rainfall excess rate (mmh^{-1}), and (iv) Manning's roughness coefficient (−). Respective outputs are overland water depth (m) and water discharge ($m^3\ s^{-1}$).

3.2. Data acquisition and elaboration

3.2.1. Overview of recorded rainfall events and observed landslides

In order to carry out SIMWE simulations, the daily rainfall intensity peaks recorded by the nearest weather station in a specific time range were considered. The weather station is located in Tenno municipality (Trento province), 1 km away from the study area as the crow flies. A specific time range was set to proceed in the analysis of weather station measurements, automatically corrected and post-processed by local services. At the indications given by the landowner about the period of landslides triggering in the vineyard, the records of rainfall values from one month before the date of each computed RPAS survey were considered. The highest rainfall intensity peaks recorded by the weather station in each considered time range were equal to 33.6 mmh^{-1} (recorded on October 2, 2019) and 7.2 mmh^{-1} (recorded on November 27, 2019), referring to continuous rainfall events lasting a total of 50 min and 390 min respectively. Fig. A. 1 shows the trend of daily cumulative rainfall (mm) and daily hourly rainfall intensity peaks (mmh^{-1}) for each month. Specific codes in R environment were adopted to extract daily rainfall intensity peaks, applying accurate transformations in the analysis of the available dataset. Annual raw meteorological data were firstly divided into monthly subgroups. Then, the extraction of both daily rainfall intensity peaks (mmh^{-1}) and cumulative rainfall values ($mmday^{-1}$) was performed through consecutive *for loops* computation. Consequently, combined plots were elaborated merging the *for loops* outcomes. In this way it was possible to organize the large amount of data collected extracting the necessary information for the purposes of this work and consequently plotting them. The *data.table* R package was necessary for data sub-setting, while the *attach(mtcars)* R function allowed us to combine each plot in a single plots-matrix as reported in Fig. A1.

During field surveys, the landslide extension and perimeter were manually measured in order to obtain a first overview of their characteristics. The width of landslides was measured with a stick meter. L1 zone observed during the first RPAS survey revealed an extension of 44 m^2, a perimeter of about 34 m and an average slope of 38°. The maximum vertical distance, between the higher point of L1 crown and the ground below, is equal to 0.85 m. The length of the paved road section located above L1 is to 11.8m, with the absence of drainage systems along it. The second RPAS survey firstly highlighted an increasing extension of L1 of more than 50 m^2 (from 44 m^2 to 98 m^2), a perimeter of about 45 m and a maximum vertical value equal to 1.20 m. Secondly, another shallow landslide was noticed (L2), covering a surface of more than 60 m^2 with a perimeter of about 40 m, a maximum vertical distance equal to 1.10 m and an average slope of 40.9°. With reference to the landslides definitions proposed by Dikau et al. (1996) and according to Thiery et al. (2017), the observed landslides can be identified as shallow translational landslides, both considering the steep slopes of the collapsed surfaces and their overall dimensions. Moreover, landslide zones mainly involved bare soil characterized by an uneven low herbaceous cover. The maximum width between each landslides' flanks is equal to 12.8 m for L1-pre, 14.10 m for L1-post, and 16.3 m for L2, while the length of the collapsed surfaces, from each landslides' crown and the respective toe, is equal to 6.3 m for L1-pre, 6.6 m for L1-post and 4.4 m for L2 (Cruden & Varnes, 1996, p. 247).

3.2.2. RPAS-SfM data acquisition and processing

In light of the aims of this work, a multi-temporal RPAS survey was performed to elaborate high-resolution Digital Elevation Models (DEMs) of the study area. The two surveys were carried out after two subsequent landslide events, using a DJI Mavic Pro® RPAS mounted with a 1/2.3″ sensor (CMOS) 12.35M effective pixels camera. Flight missions were planned using the official IOS-DJI® application. Nadir and oblique pictures were integrated to better appreciate specific features such as terraces and landslides (Rusnák et al., 2018). The positions of 23 GCPs and 10 CPs were measured through the Geomax Zenith40® GNSS receiver in RTK mode (EPSG 32632 coordinate system-WGS 84/UTM zone 32N). Agisoft

Table 1
Overview of main parameters describing the SfM point clouds and the obtain DEMs for the first RPAS survey (18 October 2019) and the second one (17 December 2019). The table shows the point cloud accuracy (described by the absolute mean of CPs residuals), point cloud precision (described by the standard deviation of CPs residuals) for the two RPAS surveys, RMSE3D total value observed during point clouds' elaboration, respectively regarding GCPs and CPs, co-registration error and RMSE values of final DEMs.

Point cloud	Point cloud accuracy (m)			Point cloud precision (m)			$RMSE_{3D}$ CPs (m)	$RMSE_{3D}$ GCPs (m)	RMSE *Co-reg. (m)*	RMSE DEM (m)
	X	y	z	x	y	z				
Survey 1	0.040	0.020	0.035	0.020	0.026	0.037	0.057	0.039	0.045	0.103
Survey 2	0.017	0.016	0.038	0.014	0.012	0.026	0.046	0.039		0.058

Metashape® software was used for point clouds generation, while point clouds post-processing was performed with Cloud Compare software (http://www.cloudcompare.org). In particular, the Statistical Outlier Removal (SOR) filter, based on the Point Cloud Library (PCL) (Rusu & Cousins, 2011) was firstly used for outliers removal. Subsequently, point clouds were manually cleaned by dividing them into regular slices along the maximum slope direction, easing the removal of noises such as residual vegetation, vineyard's rows, plants and man-made features. In this regard, despite the availability of several semi-automatic algorithms for the automatic extraction of clouds-derived terrain points, manual filtering led to a more accurate cleaning procedure. Finally, point clouds co-registration was computed through the Point Pairs Picking co-registration tool in Cloud Compare. Manholes located along the paved road section around the vineyard were considered as specific stable point's pairs in both the point clouds to be aligned. DEMs

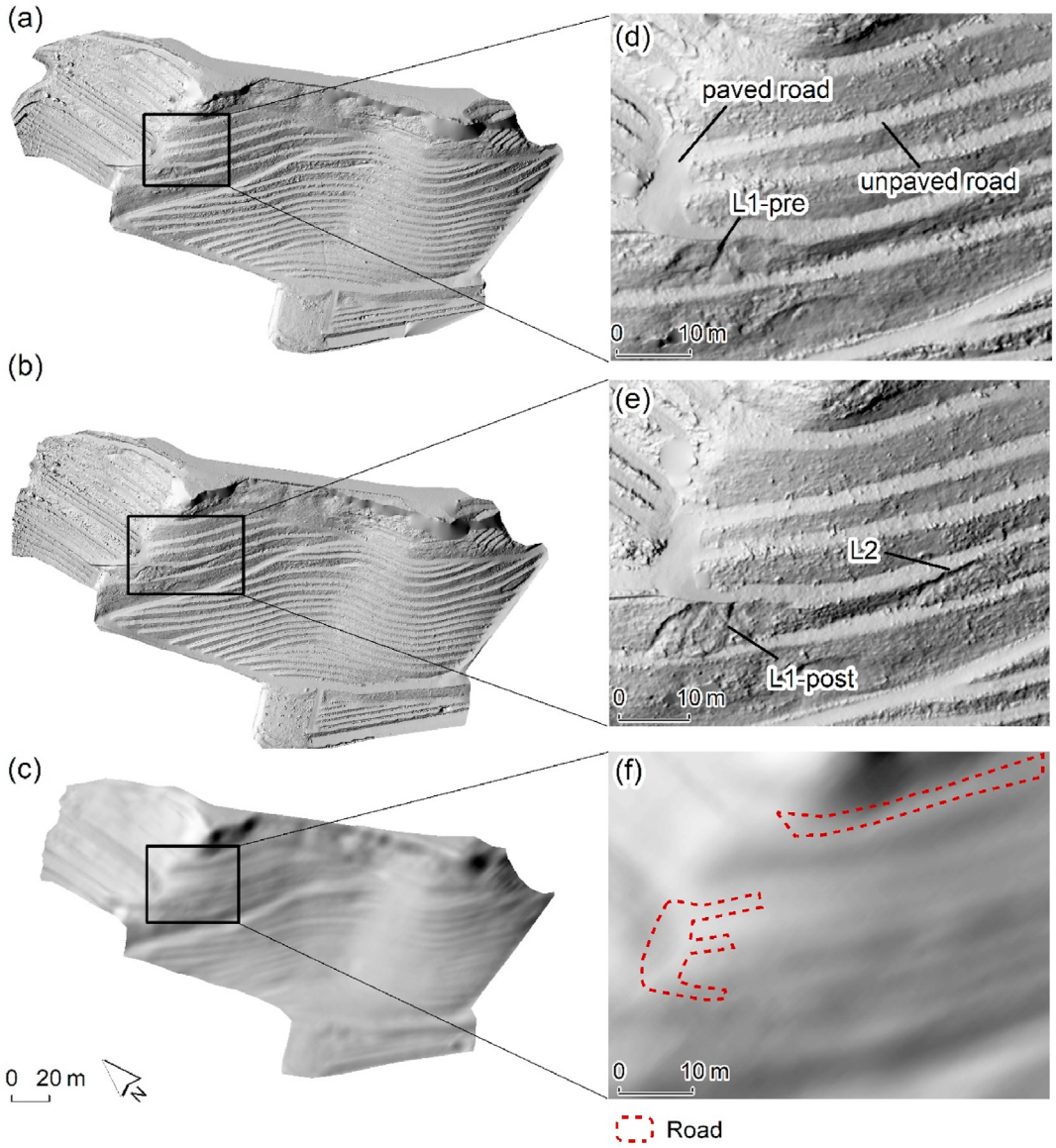

Fig. 2. Overview of shaded relief maps of each DEM obtained from the first RPAS survey (Fig. 2a), from the second one (Fig. 2b), and from the adopted smoothing procedure (Fig. 2c). The figure also shows details of each computed DEM, regarding L1-pre and the above paved road section (Fig. 2d), L1-post, L2 and the above unpaved road section (Fig. 2e) and the original location of the road in the smoothed DEM, which simulates its absence (Fig. 2f).

Table 2
Overview of SIMWE input selected for each simulation of the YesRoad-pre and YesRoad-post scenarios. In particular, the table shows Manning, infiltration rate and excess rate values considered for each land type, i.e., vineyard (V), grassland (G), bare soil (i.e., landsides zones, BS), concrete road sections (CR) and unpaved road sections (UR). Simulations 1 and 3 were computed considering the highest rainfall intensity peaks recorded by the weather station in the time range referring to the first and the second RPAS survey respectively, while simulations 2, 4, 5 and 6 were computed considering hypothetical rainfall intensity peaks.

SIMWE sim	Land type	Manning (n)	Infiltration rate (mmh^{-1})	Excess rate (mmh^{-1})
1 (7.2 mmh^{-1}) (rec)	V	0.030	37.5	0.0
	G	0.035	12.7	0.0
	BS	0.030	12.7	0.0
	CR	0.120	0.0	7.2
	UR	0.035	9.8	0.0
2 (25.0 mmh^{-1}) (sim)	V	0.030	37.5	0.0
	G	0.035	12.7	12.3
	BS	0.030	12.7	12.3
	CR	0.120	0.0	25.0
	UR	0.035	9.8	15.2
3 (33.6 mmh^{-1}) (rec)	V	0.030	37.5	0.0
	G	0.035	12.7	20.9
	BS	0.030	12.7	20.9
	CR	0.120	0.0	33.6
	UR	0.035	9.8	23.8
4 (40.0 mmh^{-1}) (sim)	V	0.030	37.5	2.5
	G	0.035	12.7	27.3
	BS	0.030	12.7	27.3
	CR	0.120	0.0	40.0
	UR	0.035	9.8	30.2
5 (60.0 mmh^{-1}) (sim)	V	0.030	37.5	22.5
	G	0.035	12.7	47.3
	BS	0.030	12.7	47.3
	CR	0.120	0.0	60.0
	UR	0.035	9.8	50.2
6 (80.0 mmh^{-1}) (sim)	V	0.030	37.5	42.5
	G	0.035	12.7	67.3
	BS	0.030	12.7	67.3
	CR	0.120	0.0	80.0
	UR	0.035	9.8	70.2

Table 3
Overview of SIMWE input selected for each simulation of the NoRoad scenario. In particular, the table shows Manning, infiltration rate and excess rate values considered for each land type, i.e., vineyard (V), grassland (G) and bare soil (i.e., landsides zones, BS). SIMWE simulations were computed adopting the same rainfall intensity peak values previously set in each YesRoad scenario.

SIMWE sim	Land type	Manning (n)	Infiltration rate (mmh^{-1})	Excess rate (mmh^{-1})
1 (7.2 mmh^{-1}) (sim)	V	0.030	37.5	0.0
	G	0.035	12.7	0.0
	BS	0.030	12.7	0.0
2 (25.0 mmh^{-1}) (sim)	V	0.030	37.5	0.0
	G	0.035	12.7	12.3
	BS	0.030	12.7	12.3
3 (33.6 mmh^{-1}) (sim)	V	0.030	37.5	0.0
	G	0.035	12.7	20.9
	BS	0.030	12.7	20.9
4 (40.0 mmh^{-1}) (sim)	V	0.030	37.5	2.5
	G	0.035	12.7	27.3
	BS	0.030	12.7	27.3
5 (60.0 mmh^{-1}) (sim)	V	0.030	37.5	22.5
	G	0.035	12.7	47.3
	BS	0.030	12.7	47.3
6 (80.0 mmh^{-1}) (sim)	V	0.030	37.5	42.5
	G	0.035	12.7	67.3
	BS	0.030	12.7	67.3

elaboration was carried out adopting the Natural Neighbour Interpolation technique, which provides a value for the unknown point according to the weight assigned to each one as a function of a proportional area, basing on a subset of surrounding points. Looking at the average point distance, the two elevation models were elaborated with a resolution equal to 15 cm, in order to efficiently appreciate geomorphological features at the hillslope scale. The analysis of errors affecting point clouds and the respective DEMs highlighted the success of the measurements in terms of accuracy and precision of the results. The point clouds' accuracy and precision were estimated by selecting 1/3 of GCPs, excluding them from data georeferencing procedure and hence considering them as check-points (CPs). Consequently, the computation of GCPs and CPs residuals was conducted (Cucchiaro et al., 2018). In this regard, the absolute mean and the standard deviation of CPs residuals describe the point cloud accuracy and precision respectively (Cucchiaro et al., 2018). The Root Mean Square Error ($RMSE_{3D}$) was computed in x, y and z directions by comparing the value of each coordinate provided by the SfM technique with the corresponding value measured by GNSS close to each GCPs and CPs. Analogously,

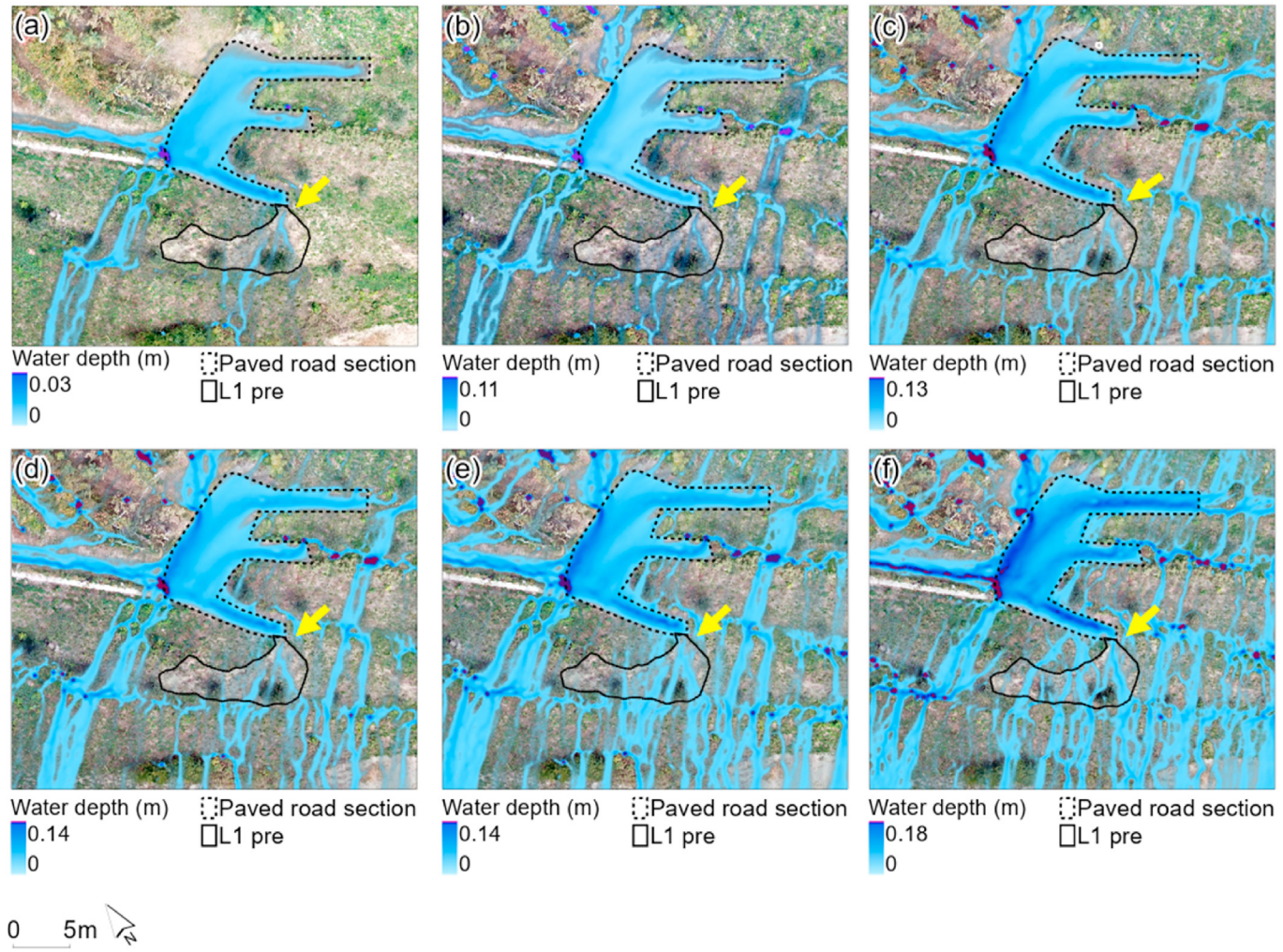

Fig. 3. Water depth (m) computed for SIMWE simulations regarding L1-pre (YesRoad scenario). In particular, the figure shows water depth simulation in function of rainfall intensity peaks equal to 7.2 mmh^{-1} (a), 25.0 mmh^{-1} (b), 33.6 mmh^{-1} (c), 40.0 mmh^{-1} (d), 60.0 mmh^{-1} (e) and 80.0 mmh^{-1} (f). Fig. 3c refers to the highest rainfall intensity peak recorded by the weather station in the considered time range, while Fig. 3a, b, d-f refer to the simulated rainfall intensity peaks. Yellow arrows indicate the main road-induced water flows deviations in the direction of L1-pre.

DEM-RMSE values were obtained. Finally, the co-registration RMSE value was obtained as a result of the adopted point clouds alignment procedure. Table 1 reports an overview of the main parameters characterizing the RPAS-derived SfM outcomes.

3.2.3. SIMWE input acquisition

Starting from each computed DEM, the flow gradient vector (given by first-order x and y partial derivates of elevation grids) was obtained through the GRASS GIS *r.slope.aspect* tool. Manning's roughness coefficients (n) were selected from literature (Bunya et al., 2010; Fernandes et al., 2017; Pijl et al., 2020). Different surface types were observed within the study area, as reported in Fig. A2. Specifically, vineyard (V), grassland (G), bare soil (i.e., landslides zones, BS), concrete road sections (CR) and unpaved road sections (UR) were noticed within the study area. Specific Manning values were adopted, setting n equal to 0.100 for vineyard, 0.035 for grass zones, 0.030 for bare soil, 0.012 for the concrete surface of the road and 0.035 for its unpaved sections. The rainfall excess rate was calculated by subtracting the infiltration rate (mmh^{-1}) from the fixed rainfall rate (mmh^{-1}, i.e., the rainfall intensity peaks recorded by the weather station for each month). Infiltration rates were estimated based on the measurement of the hydraulic conductivity for each land type and resulted equal to 37.5 mmh^{-1} for vineyard, 12.7 mmh^{-1} for grassland zones and bare soil, 9.8 mmh^{-1} for unpaved road's sections and 0 mmh^{-1} for concrete road's sections. Saturated hydraulic conductivity was calculated for each surface type using a double-ring infiltrometer with a diameter equal to 80 cm, following the outcomes presented in Lai and Ren (2007) and Fatehna et al. (2016). Field measurements of hydraulic conductivity are in line with those reported in the respective literature (Alagna et al., 2018; Biddoccu et al., 2013; Capello et al., 2019; Pijl et al., 2020).

3.3. SIMWE simulations on different scenarios

Looking at the aims of the presented research, three different scenarios were considered to investigate the role played by the road network in the deviation of water flows close to the collapsed hillslopes. A multi-temporal comparison of SIMWE simulations was computed, so as to detect the evolution of water dynamics among time. DEMs resulted from the two RPAS surveys were respectively considered (Fig. 2a and b). In the first scenario (henceforth called "*YesRoad-pre*") the first RPAS-derived DEM was used and water flows were simulated looking at the presence of the road, especially close to the collapsed surface detected during the survey. The second scenario (called "*YesRoad-post*") considered the second reconstructed DEM, characterized by an L1 evolution and L2

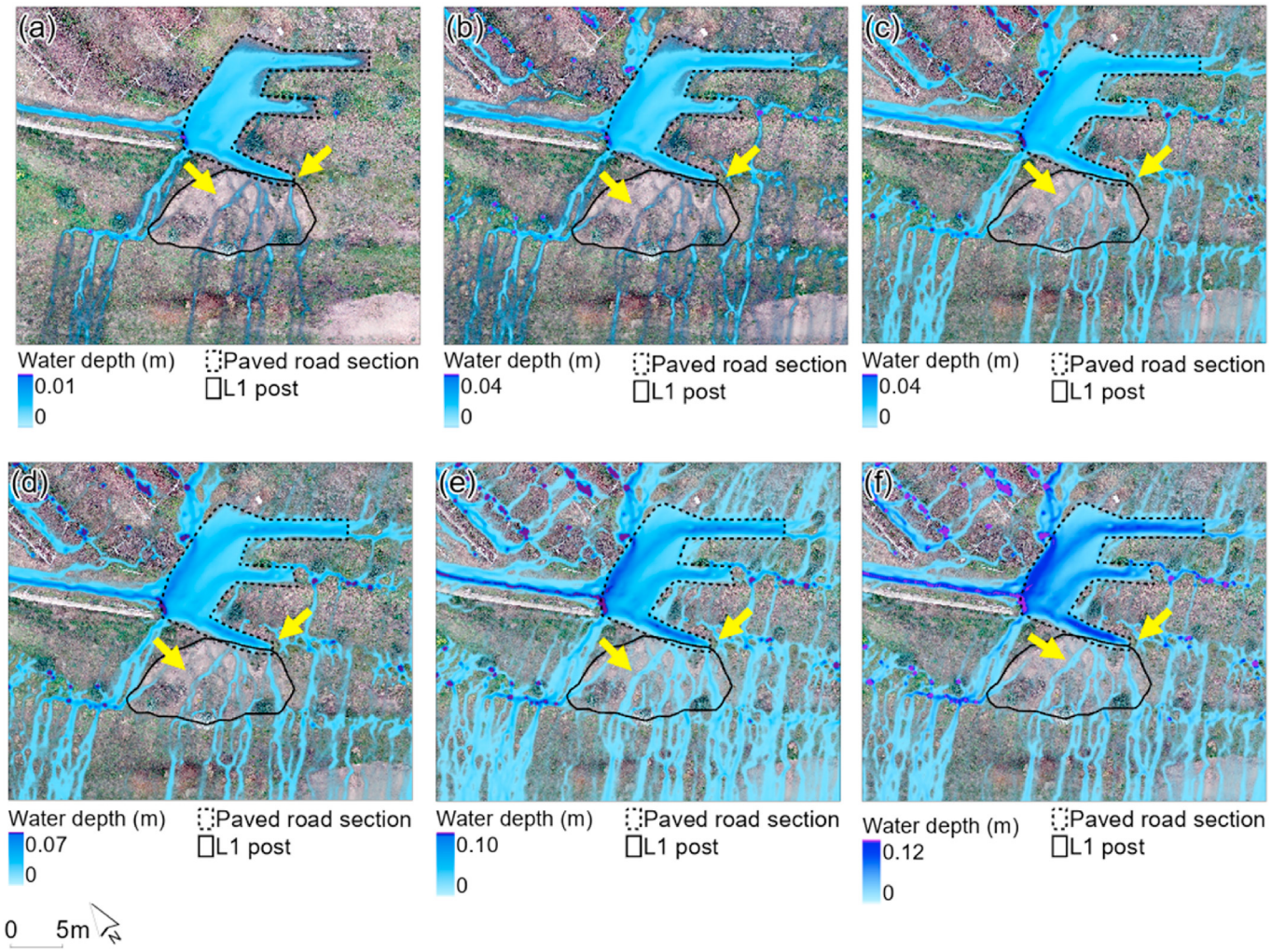

Fig. 4. Water depth (m) computed for SIMWE simulations regarding L1-post (YesRoad scenario). In particular, the figure shows water depth simulation in function of rainfall intensity peaks equal to 7.2 mmh^{-1} (a), 25.0 mmh^{-1} (b), 33.6 mmh^{-1} (c), 40.0 mmh^{-1} (d), 60.0 mmh^{-1} (e) and 80.0 mmh^{-1} (f). Fig. 4a refers to the highest rainfall intensity peak recorded by the weather station in the considered time range, while Fig. 4b–f refer to the simulated rainfall intensity peaks. Yellow arrows indicate main road induced water flows deviations in the direction of L1-post.

activation. The third scenario (named "*NoRoad*") was carried out simulating the absence of the road network within the study area (Fig. 2c). The road absence was simulated modifying each DEM through a specific smoothing approach applying the quadratic approximation introduced by Evans (1979).

$$Z = ax^2 + by^2 + cxy + dx + ey + f$$

where x, y and Z are local coordinates and parameters a to f stand for the quadratic coefficients. A moving window equal to 91 m was used in the smoothing process, so as to efficiently simulate the absence of the road network within the study area, reasonably preserving the presence of terraces (in Fig. 2c it is possible to note the light shadow of few terrace lines that are preserved after the smoothing procedure). Considering both DEMs resolution and road size, this revealed to be the most suitable value to properly smooth the road feature, also preventing an excessive reduction of DEMs size unavoidably deriving from the smoothing process. This smoothing approach was already satisfactorily tested in other contexts (see Tarolli et al., 2015).

For the *YesRoad* scenarios, the highest rainfall intensity peaks recorded by the weather station in each considered time range were firstly set in SIMWE simulations. Different tests were successively performed both decreasing and increasing rainfall intensity peaks with respect to those registered and hence modifying the excess rate respectively. Table 2 reports SIMWE input selected for each simulation of the *YesRoad* scenarios. The same values were used in each simulation of the *NoRoad* scenario, as reported in Table 3. For both the *YesRoad* and *NoRoad* scenarios, the duration of the simulations was 1 h, in agreement with the unit of measurement of the model inputs.

4. Results

4.1. Multi-temporal hydrological simulations

A 4D analysis of overland water flows dynamics was conducted in order to investigate the role of the road network in overland flows directions and quantify their alteration. The output of the model is expressed in terms of water depth of overland flows (m). The analysis was conducted considering the presence of the road (*YesRoad*) and then simulating its absence (*NoRoad*).

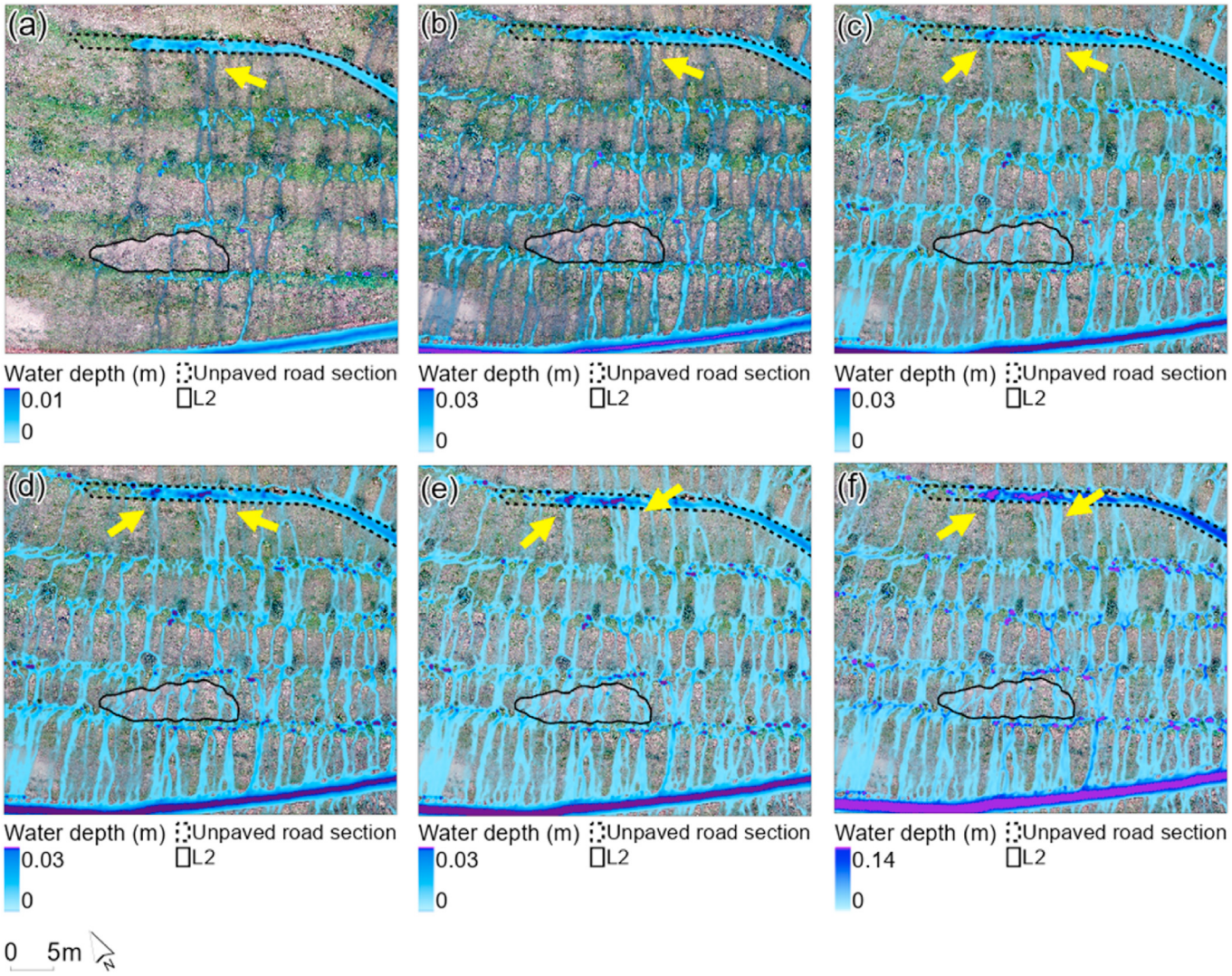

Fig. 5. Water depth (m) computed for SIMWE simulations regarding L2 (YesRoad scenario). In particular, the figure shows water depth simulation in function of rainfall intensity peaks equal to 7.2 mmh^{-1} (a), 25.0 mmh^{-1} (b), 33.6 mmh^{-1} (c), 40.0 mmh^{-1} (d), 60.0 mmh^{-1} (e) and 80.0 mmh^{-1} (f). Fig. 5a refers to the highest rainfall intensity peak recorded by the weather station in the considered time range, while Fig. 5b–f refers to the simulated rainfall intensity peaks. Yellow arrows indicate the most relevant water flows deviated by the unpaved road section located above L2, crossing the terraces downstream and intercepting the collapsed hillslope.

4.1.1. YesRoad scenarios

Fig. 3 shows water flows computed for L1-pre, in function of each rainfall peak set as input in SIMWE simulations. The figures highlight a significant increase in water depth, proportionally to the configured rainfall values. Water flows, coming from the upper terraces, intercept the paved road section located above the landslide zone. Surface runoff flows along the road since it falls from its wayside crossing the underlying collapsed hillslope. This is evident both in simulations computed looking at the recorded rainfall intensities (Fig. 3c) and in those that considered the simulated scenarios (Fig. 3a, b, d-f). The figure underlines the presence of water flows deviation at the paved road section (yellow arrows), where water is deviated downstream by the road, crossing L1-pre. Moreover, the highest values of water depth were noticed close to the left corner of the paved road, specifically where water deviates in the direction of the terraces located further down. As rainfall values increase, water depth reaches gradually higher values up to a maximum of over 0.13 m and 0.18 m, regarding the simulations considering recorded (Fig. 3c) and simulated (Fig. 3a, b, d-f) rainfall intensity peaks respectively. Finally, part of the incoming water is deviated by the road on the left side, along an unpaved section that partially conveys it outside the investigated landslide-prone area.

Fig. 4 represents SIMWE simulations elaborated for L1-post, therefore considering the second RPAS-derived DEM, in function of progressively increasing rainfall intensity peaks values. The figure underlines the deviation of overland flows due to the presence of the paved road, which is responsible for changes in water directions and increasing water depth proportionally to the rainfall intensity peaks. L1-post is crossed by water that coming from the upper hillslopes, is then deviated by the road. The unaltered hillslope located close to L1 is likewise involved in road-altered water flows which pass through it. The highest water depth values were noticed close to the left corner of the paved road section above L1-post, with a maximum of 0.01 m and 0.12 m regarding the simulations considering recorded (Fig. 4a) and simulated (Fig. 4b–f) rainfall intensity peaks respectively.

Fig. 5 represents the simulation included in the *YesRoad* scenario looking to L2, observed during the second RPAS survey. Water flows

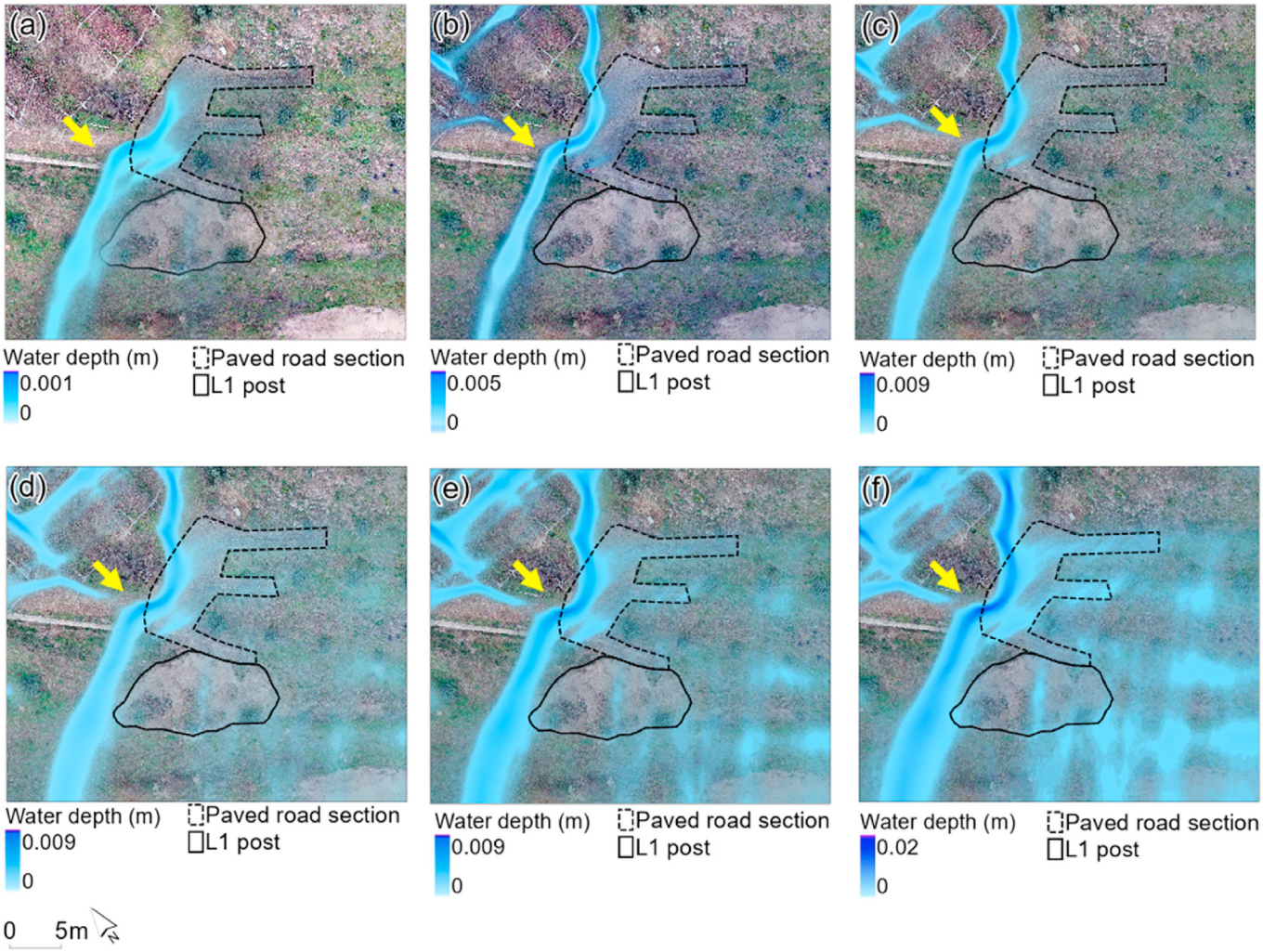

Fig. 6. Water depth (m) computed for SIMWE simulations regarding L1 (NoRoad scenario). In particular, the figure shows water depth simulation in function of rainfall peaks equal to 7.2 mmh^{-1} (a), 25.0 mmh^{-1} (b), 33.6 mmh^{-1} (c), 40.0 mmh^{-1} (d), 60.0 mmh^{-1} (e) and 80.0 mmh^{-1} (f). SIMWE simulations were computed adopting the same rainfall intensity peaks values previously set in the YesRoad scenarios. Yellow arrows indicate the highest water depth values involving an unaltered hillslope close to L1.

deviations are more significant as the rainfall increase, with water depth values ranging from 0.01 m (Fig. 5a) up to a maximum of 0.14 m regarding the last simulation elaborated considering the hypothesized rainfall intensity peaks (Fig. 5f). Moreover, the figure shows the presence of high water depth along the unpaved road section located above L2, proportionally to the increasing rainfall values. Yellow arrows indicate the most evident water flows that moving along the roadway deviate downstream across terraces, until intercepting the landslide zone more significantly as the rainfall intensity increases.

Looking at L1, the comparison of SIMWE simulations computed for the *YesRoad-pre* and *YesRoad-post* scenarios (Figs. 3–4) strongly proves a connection between road presence and water flows deviation towards L1 zone. Analogously, the presence of water flows diversion above L2 (Fig. 5) suggests as unpaved road sections can be similarly responsible for notable alterations of water overland flows.

4.1.2. NoRoad scenario

Fig. 6 reveals the absence of significant changes in water flows involving L1. Simulations identify the presence of the highest water depth values close to the left part of the paved road section located above the landslide (yellow arrows). As the rainfall increases, the water depth reaches higher values until a maximum of 0.02 m. L1 is not crossed by the water, which only drains from the left part of the road through the unaltered hillslope near the collapsed surface. Maximum water depth was noticed close to the left corner of the paved section of the road, further underlining the concentration of water toward the unaltered hillslope located near L1. Water depth increases proportionally to the rainfall value set as input in the model, without involving the landslide zone.

Finally, Fig. 7 represents the simulations of water flows assuming the absence of the road, focusing on L2. As the rainfall increases, the landslide area reveals not to be crossed by the water, with maximum water depth values in the order of millimetres.

4.2. Water depth comparison and statistical validation

Looking at the purposes of this research, a quantification of water depth along the road sections was performed. In this regard, 25 control points were placed at equal distances from each other on both paved and unpaved road sections, respectively located above L1 and L2, for a total of 50 control points (Fig. A3). For each simulation of the three scenarios, water depth values were extracted in correspondence of each point obtaining a total of 900 water depth

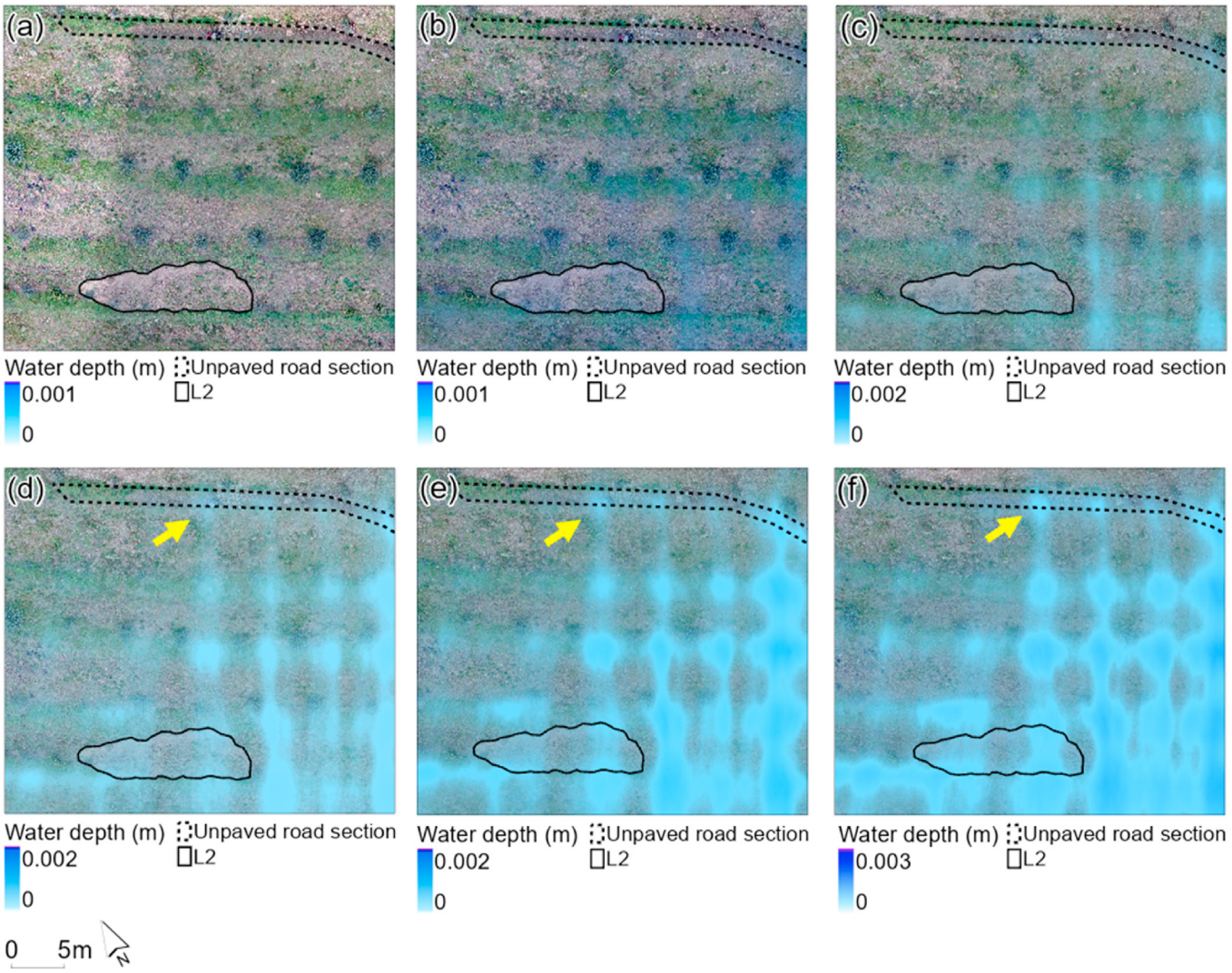

Fig. 7. Water depth (m) computed for SIMWE simulations regarding L2 (NoRoad scenario). In particular, the figure shows water depth simulation in function of rainfall intensity peaks equal to 7.2 mmh^{-1} (a), 25.0 mmh^{-1} (b), 33.6 mmh^{-1} (c), 40.0 mmh^{-1} (d), 60.0 mmh^{-1} (e) and 80.0 mmh^{-1} (f). SIMWE simulations were computed adopting the same rainfall intensity peaks values previously set in the YesRoad scenarios. Yellow arrows indicate the highest water depth values, regarding assumed water overland flows crossing L2.

measures.

Boxplots in Fig. 8 show water depth extracted from each control point placed along the paved road section above L1-pre and L1-post (Fig. 8a and b) and on the unpaved road section above L2 (Fig. 8c). Each figure compares the different values of water depth considering both *YesRoad* and *NoRoad* scenarios. Looking at the road sections above L1 and L2 (Fig. 8a and b and Fig.8c respectively), water depth extracted from each point increases proportionally to the rainfall intensity peaks set as input in SIMWE simulations. In contrast, concerning the simulations computed assuming the absence of the road, points-derived water depth values are around 0 m for both L1 and L2, regardless of the increasing rainfall intensity peaks.

The influence of the road network on the overland flows deviation towards the collapsed surfaces was then investigated by computing a topographic cross sections of water depth values for each landslide zones. In this regard, water depth values for *YesRoad* and *NoRoad* scenarios were extracted along a line tracked crosswise L1 and L2 respectively. Line plots in Fig. 9 show cross sections outcomes for each scenario. Looking at the presence and at the assumed absence of the road, the comparison of water depth cross sections extracted for L1-pre (Fig. 9a–b) L1-post (Fig. 9c–d) and L2 zone (Fig. 9e–f) highlights the role played by the road in water flows diversion toward the collapsed hillslopes.

The comparison of cross-sections computed for *YesRoad* and *NoRoad* scenarios further proves as the assumed absence of the road strongly influences the amount of water crossing the collapsed surface.

Statgraphics® software and specific codes implemented in R environment were used to perform statistical analysis. Statistical hypothesis testing was carried out, through the computation of both normality test and two-sample *t*-test assuming unequal variances. Normality distribution of data was firstly checked through the application of the Shapiro-Wilk normality test. In this regard, since Shapiro-Wilk-derived p-values resulted greater than the considered significance level (alpha equal to 0.05), water depth values extracted from control points placed along the road sections above L1-pre, L1-post and L2 were found to be normally distributed. Statistical differences between the presence and the assumed absence of the road network, in terms of water accumulation along its detected sections, were investigated. Therefore, the null

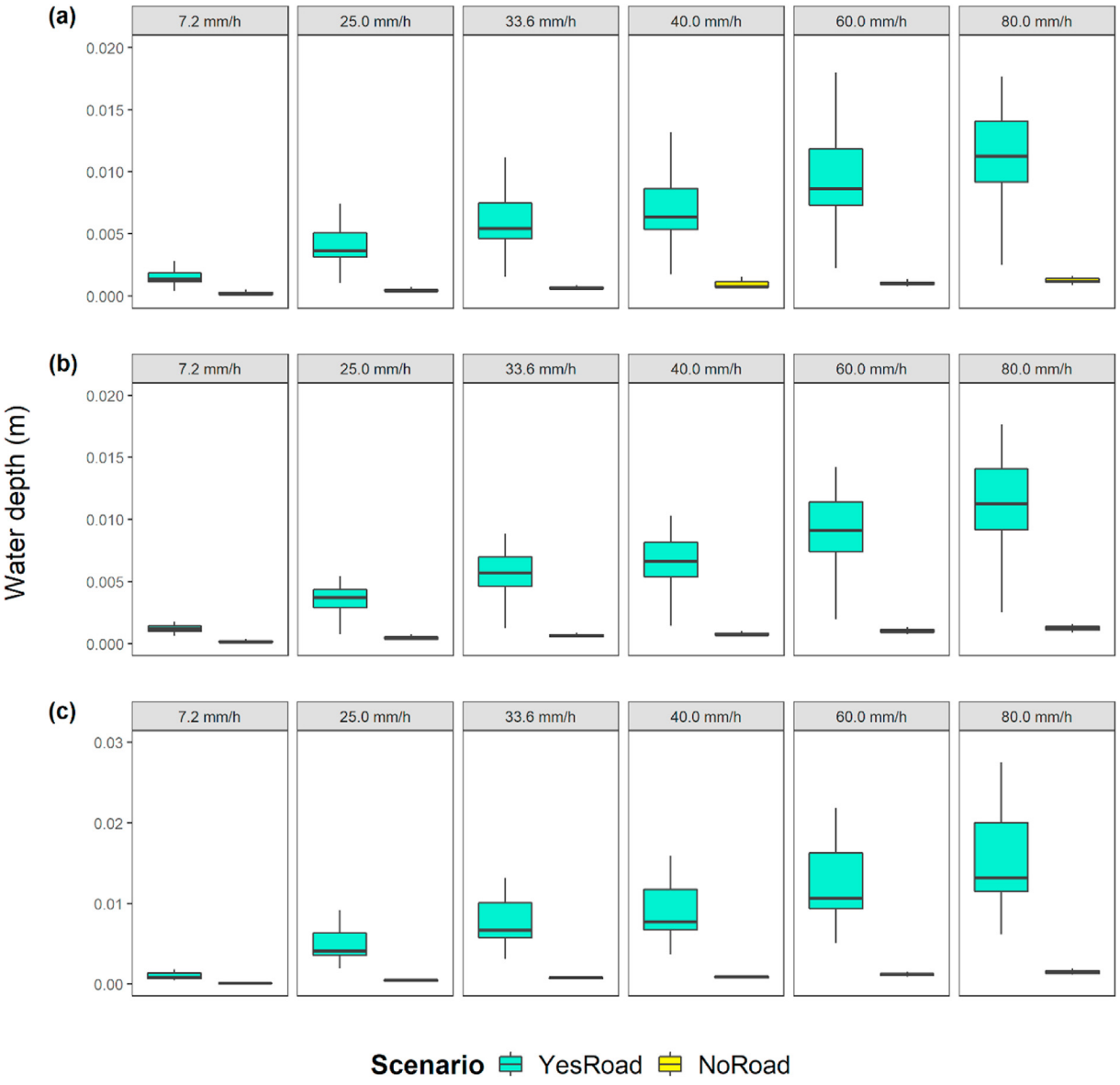

Fig. 8. Boxplots of water depth values extracted from each control point located along the paved and the unpaved road sections above L1-pre (a), L1-post (b) and L2 (c). The figure shows the comparison between water depth values acquired from each control point for YesRoad and NoRoad scenarios regarding each computed SIMWE simulation. Outliers have been removed to propose a clearer visualization of the graphics.

hypothesis (H_0) and the alternative hypothesis (H_1) were identified. H_0 assumed that the presence of the road does not affect water accumulation and deviation in the direction of the landslides-prone zones, while H_1 considered the effective role played by the road in increasing water depth along with it and therefore in the likely activation of the observed shallow landslides. Moreover, two-tail p values (alpha equal to 0.05) were calculated to further support the outcomes of the statistical analysis. The following tables show the results of the computed statistical analysis regarding water depth values extracted from each control point along road sections above L1-pre (Table A1), L1-post (Table A2), and L2 (Table A3). Looking at the following tables, since t values are greater than t-statistic, H_0 is rejected in favor of H_1 for all the scenarios. This is also confirmed by the computation of *p*-values, which are highly minor than the significance level, thus proving that the considered sample gives reasonable evidence to support the alternative hypothesis.

5. Discussion

This work proposes an analysis of road influence on water flows alteration in a terraced vineyard affected by shallow landslides. For this purpose, a multi-temporal hydrological analysis was computed through the adoption of a specific hydrological model in the simulation of overland flow dynamics on the landslides-prone hillslopes among time. In this perspective, our work further highlighted the efficiency of RPAS-based SfM multi-temporal surveys in the investigation of the presented issue, in line with the application of such a technology in agricultural contexts recently proposed by Tucci et al. (2019), Yamazaki et al. (2019), Meinen and Robinson (2020) and Mauri et al. (2021). Thanks to the adoption of this photogrammetric technique, the creation of high-resolution DEMs allowed to perform a detailed hydrological analysis at the hillslope scale, differently from similar investigations conducted at the watershed scale (Arnone et al., 2011; Jebur et al., 2014) and on wider one (De Vita et al., 2013; Yang et al., 2019; Zhao et al., 2019).

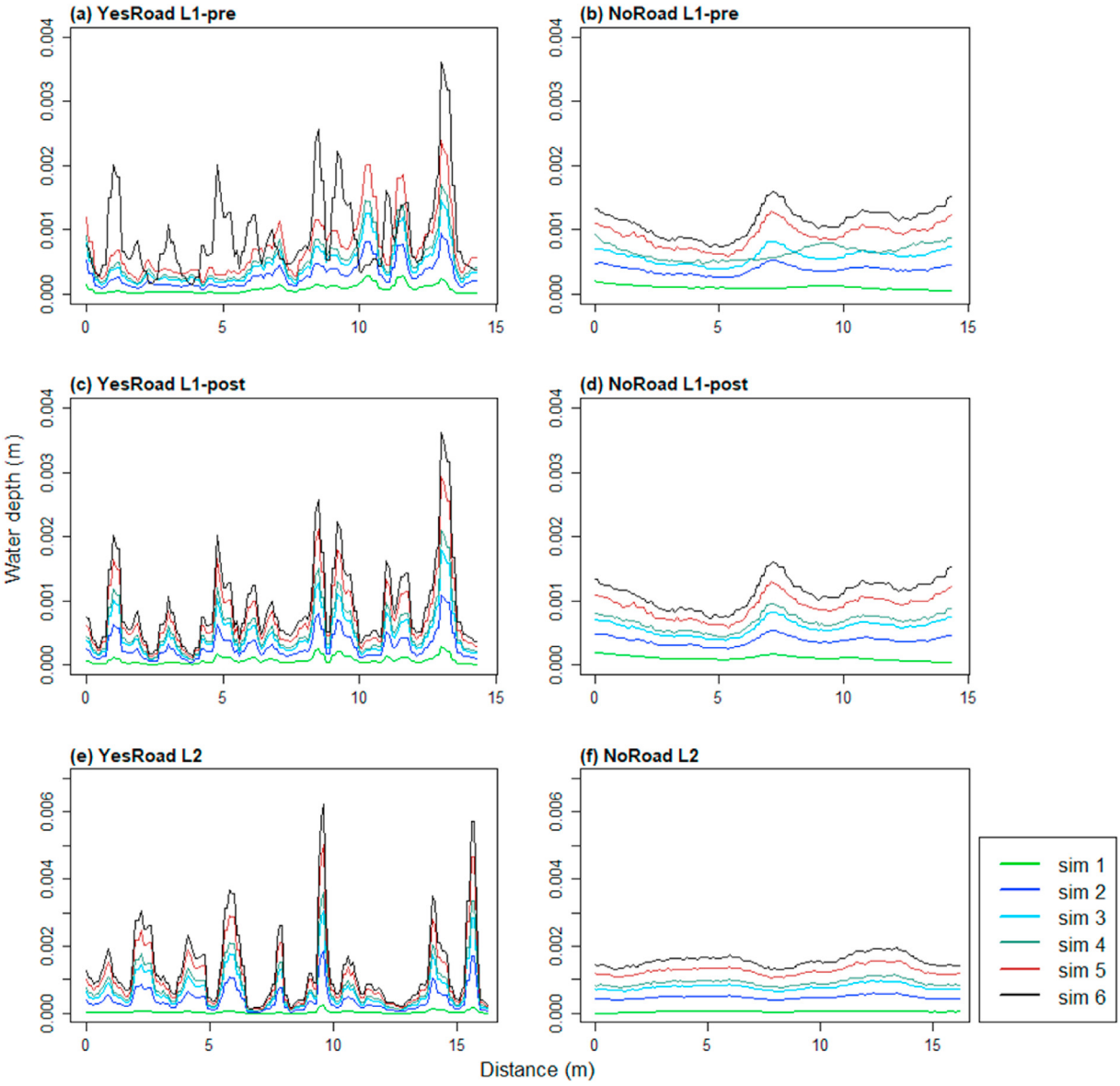

Fig. 9. Line plots showing water depth cross-sections computed for each simulation of the YesRoad and NoRoad scenarios. In particular, the figure shows water depth cross-sections elaborated both looking at the presence of the road and its assumed absence for L1-pre (a–b), L1-post (c–d) and L2 (e–f).

Several studies have been carried out about water dynamics on landslide-prone steep slopes, focusing on spatio-temporal dynamics of soil water content (Arnone et al., 2011), rainfall influence on landslides activation (Collins et al., 2004; Dai & Lee, 2001; Kefeer et al., 1987), changes in subsurface water and soil properties (Bogaard & Greco, 2016; Ray & Jacobs, 2007; Yang et al., 2019; Zhao et al., 2019), landslide hydrology investigation (Smith, Goodrich, & Quinton, 1995) and critical rainfall threshold evaluation (Guzzetti et al., 2007; Brunetti et al., 2010; Brendan, Mitasova, Petrasova, & Vaclav, 2019). In this context, even though the availability of many investigations of the role played by roads and trails in land degradation phenomena like erosion processes (Elliot et al., 1999; MacDonald et al., 2001; Salesa et al., 2019; Yu et al., 2021) and landslides occurrence (Fu et al., 2010; Penna et al., 2014; Sidle & Ziegler, 2012; Tarolli et al., 2021), our research distinguishes from those available in the respective literature in that it proposes an innovative comparison of road-water-landslides interaction among time at centimetres scale, in function of both recorded and simulated rainfall intensity peaks.

The multi-temporal comparison of SIMWE simulations for the *YesRoad* and *NoRoad* scenarios was suitable for the investigation of the role played by the road network in the alteration of superficial water flows close to the collapsed surfaces. In this regard, the assumed absence of the road and the corresponding hydrological simulations proved its active contribution in diverting overland water directions. Differently from the common applications of SIMWE (Cencetti et al., 2005; Fernandes et al., 2017; Koco, 2011; Pijl et al., 2020) the multi-temporality that distinguishes the adoption of the model is completely novel, as well as the investigation of superficial water dynamics looking at the assumed absence of infrastructures. In this regard, our work fills the gap in the scientific knowledge regarding the possibility to perform such a low-cost, high-resolution, multi-temporal hydrological analysis at a hillslope scale.

Looking at the examined study area, our research also suggests as the absence of drainage systems along the road sections located

above the shallow landslides has a relevant influence on runoff dynamics on the roadway. Similar outcomes have been proposed by Mulder et al. (1994), Vlotman et al. (2001), Needelman et al. (2007), Mrvìk and Bomont (2012) and Skaggs et al. (2012), who investigated the role played by drainage systems on efficient water management and land degradation control in agricultural environments.

Furthermore, the simulation of the absence of road so as to highlight its role in the alteration of water flow directions close to the slope failure further proved the capability of the SIMWE model in the description of the interaction between road network and water runoff dynamics in hydrological terms.

6. Conclusions

This work proposes a multi-temporal analysis of road-induced overland flow alteration in an agricultural terraced area characterized by the activation of shallow landslides. RPAS-based SfM technique allowed to obtain high-resolution DEMs, which served as a base to perform a 4D hydrological analysis through an innovative application of the SIMWE model. Simulations under the *NoRoad* scenario were also performed, smoothing the RPAS-derived DEM and investigating water dynamics in function of the recorded and the assumed rainfall intensity peaks set as input in the model. Our work represents a solid starting point for future investigations on a wider scale. This work also underlined as the presence of rural roads within a steep slope agricultural context can be particularly critical in terms of runoff deviation towards collapsed hillslopes. In this regard, the proposed methodology can be considered as a useful tool for obtain hydrologic maps or modeling of land degradation phenomena affecting agricultural areas, in order to identify those zones that could be potentially involved in the occurrence of future land degradation processes (eg., slope failures).

More investigations could be undertaken to deeply investigate the dynamics of surface water flows assuming the presence of drainage systems (e.g., ditches) along the roadway, as well as focusing on the role played by specific road characteristics in both runoff deviation and landslides activation. The multi-temporal comparison of SIMWE simulations reasonably suggests that the absence of drainage systems might represent a primary factor in the alteration of water runoff, which in turn could be involved in consequential landslides triggering.

Specific interventions such as hillslopes stabilization, soil management and restoration, as well as the design of efficient drainage systems could be carried out starting from the comparison of hydrological simulations. Analogously, the proposed application of the SIMWE model could be useful in figuring out critical rainfall thresholds related to the occurrence of land degradation events such as landslides and erosion processes, focusing on detailed planning of mitigation interventions at plot scale able to reduce the occurrence of future land degradation phenomena. Finally, multi-temporal hydrological simulations could allow to conduct specific geotechnical investigation regarding shallow landslides activation and perform slope stability analysis, in order to properly prove the role played by the road network in the occurrence of these land degradation phenomena. The integration of such detailed studies would be a solid starting point for the identification of those areas that are more prone to landslide occurrence.

Declaration of competing interest

None.

Acknowledgments

This research was partly founded by the University of Padova research project DOR2079232/20 “Analysis of soil erosion and surface ponding in the agricultural context”. The authors kindly thank Gabriele Bombardelli and “Acetaia del Balsamico Trentino” farm for providing the study area for the research. The authors thank the anonymous reviewers for their useful suggestions that helped us to improve our research.

Appendix A. Supplementary data

Supplementary data to this article can be found online at https://doi.org/10.1016/j.iswcr.2021.07.004.

References

Alagna, V., Di Prima, S., Rodrigo-Comino, J., Iovino, M., Pirastru, M., Keesstra, S. D., Novara, A., & Cerdà, A. (2018). The impact of the age of vines on soil hydraulic conductivity in vineyards in eastern Spain. *Water, 10*.

Arnone, E., Noto, L. V., Lepore, C., & Bras, R. L. (2011). Physically-based and distributed approach to analyze rainfall-triggered landslides at watershed scale. *Geomorphology, 133*, 121–131. https://doi.org/10.1016/j.geomorph.2011.03.019

Bajocco, S., De Angelis, A., Perini, L., Ferrara, A., & Salvati, L. (2012). The impact of land use/land cover changes on land degradation dynamics: a Mediterranean case study. *Environmental Management, 49*, 980–989. https://doi.org/10.1007/s00267-012-9831-8

Biddoccu, M., Ferraris, S., Cavallo, E., Opsi, F., Previati, M., & Canone, D. (2013). *Procedia Environmental Sciences, 19*, 351–360.

Bogaard, T. A., & Greco, R. (2016). Landslide hydrology: From hydrology to pore pressure. *Wiley Interdisciplinary Reviews: Water, 3*, 439–459. https://doi.org/10.1002/wat2.1126

Brendan, A. H., Mitasova, H., Petrasova, A., & Vaclav, P. (2019). r.sim.terrain 1.0: a landscape evolution model with dynamic hydrology. *Geoscientific Model Development, 12*, 2837–2854.

Brunetti, M. T., Peruccacci, S., Rossi, M., Luciani, S., Valigi, D., & Guzzetti, F. (2010). Rainfall thresholds for the possible occurrence of landslides in Italy. *Nat. Hazards Earth. Syst., 10*, 447–458.

Bunya, S., Dietrich, J. C., Westerink, J. J., Ebersole, B. A., Smith, J. M., Atkinson, J. H., Jensen, R., Resio, D. T., Luettich, R. A., Dawson, C., Cardone, V. J., Cox, A. T., Powell, M. D., Westerink, H. J., & Roberts, H. J. (2010). A high-resolution coupled riverine flow, tide, wind, wind wave, and storm surge model for southern Louisiana and Mississippi. Part I: Model development and validation. *Monthly Weather Review, 138*, 345–377. https://doi.org/10.1175/2009MWR2906.1

Capello, G., Biddoccu, M., Ferraris, S., & Cavallo, E. (2019). *Effects of tractor passes on hydrological and soil erosion processes in tilled and grassed vineyards* (Vol. 11). Water.

Cencetti, C., De Rosa, P., Fredduzzi, A., & Marchesini, I. (2005). Erosione dei suoli: Applicazioni tramite il software GRASS GIS. *Giornale Di Geologia Applicata, 2*, 196–202.

Collins, B. D., & Znidarcic, D. (2004). Stability analyses of rainfall induced landslides. *Journal of Geotechnical and Geoenvironmental Engineering, 130*, 362–372. https://doi.org/10.1061/(asce)1090-0241(2004)130:4(362)

Cruden, D. M., & Varnes, D. J. (1996). Landslide types and processes. *Landslides: Investigation and mitigation*. Transportation Research Board: Special Report - National Research Council.

Dai, F. C., & Lee, C. F. (2001). Frequency-volume relation and prediction of rainfall-induced landslides. *Engineering Geology, 59*, 253–266.

Davison, L., Springman, S., & Wood, D. M. (2000). *Pore water pressure*. University of the West of England. http://environment.uwe.ac.uk/geocal/SoilMech/water/water.htm.

De Vita, P., Napolitano, E., Godt, J. W., & Baum, R. L. (2013). Deterministic estimation of hydrological thresholds for shallow landslide initiation and slope stability models: Case study from the Somma-Vesuvius area of southern Italy. *Landslides, 10*, 713–728. https://doi.org/10.1007/s10346-012-0348-2

Dikau, R., Brunsden, D., Shrott, L., & Ibsen, M. L. (1996). In R. Dikau, D. Brunsden, L. Schrott, & M. L. Ibsen (Eds.), *Landslides recognition, identification, movement and causes*. New York: John Wiley & Sons, ISBN 978-0-471-96477-3.

Eker, R., & Aydin, A. (2014). Assessment of forest road conditions in terms of landslide susceptibility: A case study in yığılca forest directorate (Turkey). *Turkish Journal of Agriculture and Forestry, 38*(2), 281–290. https://doi.org/10.3906/tar-1303-12

Elliot, W. J., Foltz, R. B., & Luce, C. H. (1999). Modeling low-volume road erosion. *Transportation Research Record, 1652*, 244–249.

Evans, I. S. (1979). An integrated system of terrain analysis and slope mapping: Final Report. *Geomorphology, 36*, 274–295.

Fagnano, M., Diodato, N., Alberico, I., & Fiorentino, N. (2012). An overview of soil erosion modelling compatible with RUSLE approach. *Rend. Fis. Acc. Lincei, 23*, 69–80.

Fatehnia, M., Tawfiq, K., & Ye, M. (2016). Estimation of saturated hydraulic conductivity from double-ring infiltrometer measurements. *European Journal of Soil Science, 67*, 135–147.

Fernandes, J., Bateira, C., Soares, L., Faria, A., Oliveira, A., Hermenegildo, C., Moura, R.,

& Gonçalves, J. (2017). SIMWE model application on susceptibility analysis to bank gully erosion in Alto Douro Wine Region agricultural terraces. *Catena, 153*, 39–49.
Flanagan, D. C., & Nearing, M. A. (1995). *Water erosion prediction Project: Hillslope profile and watershed model documentation*. West Lafayette, Indiana: USDA-Agricultural Research Service, National Soil Erosion Research Laboratory. NSERL Report No.10.
Fu, B., Newhama, L. T. H., & Ramos-Scharròn, C. E. (2010). A review of surface erosion and sediment delivery models for unsealed roads. *Environmental Modelling & Software, 25*, 1–14.
Gallage, C., Abeykoon, T., & Uchimura, T. (2021). Instrumented model slopes to investigate the effects of slope inclination on rainfall-induced landslides. *Soils and Foundations, 61*, 160–174.
Gollin, D., & Rogerson, R. (2010). *Agriculture, roads, and economic development in Uganda*. NBER Working Paper. December 2009.
Guzzetti, F., Peruccacci, S., Rossi, M., & Stark, C. P. (2007). Rainfall thresholds for the initiation of landslides in central and southern Europe. *Meteorology and Atmospheric Physics, 98*, 239–267.
Harp, E. L., Wells, W. G., II, & Sarimento, J. G. (1990). Pore pressure response during failure in soils. *The Geological Society of America Bulletin, 102*, 428–438.
Jebur, M. N., Pradhan, B., & Tehrany, M. S. (2014). Optimization of landslide conditioning factors using very high-resolution airborne laser scanning (LiDAR) data at catchment scale. *Remote Sensing of Environment, 152*, 150–165. https://doi.org/10.1016/j.rse.2014.05.013
Keefer, D. K., Wilson, R. C., Mark, R. K., Brabb, E. E., Brown, W. M., Ellen, S. D., Harp, E. L., Wieczorek, G. F., Alger, C. S., & Zatkin, R. S. (1987). Real-time landslide warning during heavy rainfall. *Science, 238*, 921–925. https://doi.org/10.1126/science.238.4829.921
Koco, S. (2011). Simulation of gully erosion using the SIMWE model and GIS. *Landform Analysis, 17*, 81–86.
Lai, J., & Ren, L. (2007). Assessing the size dependency of measured hydraulic conductivity using double-ring infi ltrometers and numerical simulation. *Soil Science Society of America Journal, 71*(6), 1667–1675.
López-Vicente, M., Nadal-Romero, E., & Cammeraat, E. L. H. (2017). Hydrological connectivity does change over 70years of abandonment and afforestation in the Spanish pyrenees. *Land Degradation & Development, 28*, 1298–1310.
Louwagie, G., Gay, S. H., Sammeth, F., & Ratinger, T. (2011). The potential of European Union policies to address soil degradation in agriculture. *Land Degradation & Development, 22*(1), 5–17. https://doi.org/10.1002/ldr.1028
MacDonald, L. H., Sampson, R. W., & Anderson, D. M. (2001). Runoff and road erosion at the plot and road segment scales, St John, US Virgin Islands. *Earth Surface Processes and Landforms, 26*(3), 251–272.
Marion, J. L., & Leung, Y. F. (2004). *Environmentally sustainable trail management*. https://doi.org/10.1079/9780851998107.0229. Environmental Impacts of Ecotourism.
Mauri, L., Sallustio, L., & Tarolli, P. (2019). The geomorphologic forcing of wild boars. *Earth Surface Processes and Landforms, 44*(10). https://doi.org/10.1002/esp.4623
Mauri, L., Straffelini, E., Cucchiaro, S., & Tarolli, P. (2021). UAV-SfM 4D mapping of landslides activated in a steep terraced agricultural area. *Journal of Agricultural Engineering, 52*(1). https://doi.org/10.4081/jae.2021.1130
Meinen, U. B., & Robinson, T. D. (2020). *Mapping erosion and deposition in an agricultural landscape: Optimization of UAV image acquisition schemes for SfM-MVS. 239*. Remote Sensing of Environment.
Mitasova, H., Barton, C. M., Ullah, I., Hofierka, J., & Harmon, R. S. (2013). GIS-based soil erosion modeling. In *Treatise on geomorphology* (Vol. 3, pp. 228–258). Elsevier Inc.. *3*, 228–258.
Mitasova, H., Thaxton, C., Hofierka, J., McLaughlin, R., Moore, A., & Mitas, L. (2004). Path sampling method for modeling overland water flow, sediment transport, and short term terrain evolution in Open Source GIS. In C. T. Miller, M. W. Farthing, V. G. Gray, & G. F. Pinder (Eds.), *Proceedings of the XVth international conference on computational M* (pp. 1479–1490). Elsevier.
Mrvìk, O., & Bomont, S. (2012). In S. Landslides, & Mambretti (Eds.), *Experience with treatment of road structure landslides by innovative methods of deep drainage*.
Mulder, G. J., Luijten, C. J. L. M., & Schouten, C. P. (1994). Case study: Modelling the impact of a drainage-system along a depressed roadbed and the resulting risks to agriculture. *Future Groundwater Resources at Risk, 222*, 61–70.
Needelman, B. A., Kleinman, P. J. A., Strock, J. S., & Allen, A. L. (2007). Improved management of agricultural drainage ditches for water quality protection: An overview. *Journal of Soil and Water Conservation, 62*, 171–178.
Pamar, H. V. (2014). In *Agricultural drainage engineering: Field and laboratory manual*. Scientific Publishers.
Penna, D., Borga, M., Aronica, G. T., Brigandi, G., & Tarolli, P. (2014). The influence of grid resolution on the prediction of natural and road-related shallow landslides. *Hydrology and Earth System Sciences, 18*, 2127–2139.
Pijl, A., Reuter, L. E. H., Quarella, E., Vogel, T. A., & Tarolli, P. (2020). GIS-based soil erosion modelling under various steep-slope vineyard practices. *Catena, 193*, Article 104604. https://doi.org/10.1016/j.catena.2020.104604
Ray, R. L., & Jacobs, J. M. (2007). Relationships among remotely sensed soil moisture, precipitation and landslide events. *Natural Hazards, 43*, 211–222. https://doi.org/10.1007/s11069-006-9095-9
Romm, J. (2011). Desertification: The next dust bowl. *Nature, 478*, 450–451.
Rusnák, M., Sládek, J., Kidová, A., & Lehotský, M. (2018). Template for high-resolution river landscape mapping using UAV technology. *Measurement, 115*, 139–151.
Rusu, R. B., & Cousins, S. (2011). 3d is here: Point cloud library (pcl). *EEE International Conference on Robotics and Automation, 1–4*.
Salesa, D., Terol, E., & Cerdà, A. (2019). Soil erosion on the " el portalet " mountain trails in the eastern iberian peninsula. *The Science of the Total Environment, 661*, 504–513.
Sidle, R. C., Ghestem, M., & Stokes, A. (2014). Epic landslide erosion from mountain roads in Yunnan, China-challenges for sustainable development. *Natural Hazards and Earth System Sciences, 14*(11), 3093–3104. https://doi.org/10.5194/nhess-14-3093-2014
Sidle, R. C., & Ziegler, A. D. (2012). The dilemma of mountain roads. *Nature Publishing Group, 5*(7), 437–438. https://doi.org/10.1038/ngeo1512
Sidle, R. C., Ziegler, A. D., Negishi, J. N., Rahim, A., Siew, R., & Turkelboom, F. (2006). Erosion processes in steep terrain —truths , myths , and uncertainties related to forest management in Southeast Asia. *Forest Ecology and Management, 224*, 199–225. https://doi.org/10.1016/j.foreco.2005.12.019
Skaggs, R. W., Norman, R. F., & Evans, R. O. (2012). Drainage water management. *Journal of Soil and Water Conservation, 67*, 167A–172A.
Smith, R. E., Goodrich, D. C., & Quinton, J. N. (1995). Dynamic, distributed simulation of watershed erosion: The KINEROS2 and EUROSEM models. *Journal of Soil and Water Conservation, 14*, 533–538.
Tarolli, P., Pijl, A., Cucchiaro, S., & Wei, W. (2021). *Slope instabilities in steep cultivation systems: Process classification and opportunities from remote sensing*. Land Degradation & Development. https://doi.org/10.1002/ldr.3798
Tarolli, P., Sofia, G., Calligaro, S., Prosdocimi, M., Preti, F., & Dalla Fontana, G. (2015). Vineyards in terraced landscapes: New opportunities from lidar data. *Land Degradation & Development, 26*, 92–102. https://doi.org/10.1002/ldr.2311
Tarolli, P., & Straffelini, E. (2020). Agriculture in hilly and mountainous landscapes: threats, monitoring and sustainable management. *Geography and Sustainability, 1*(1), 70–76. https://doi.org/10.1016/j.geosus.2020.03.003
Thiery, Y., Vandromme, R., Maquaire, O., & Bernardie, S. (2017). Landslide susceptibility assessment by EPBM (expert physically based model): Strategy of calibration in complex environment. *Proceedings of World Landslide Forum, 4*.
Tucci, G., Parisi, E. I., Castelli, G., Errico, A., Corongiu, M., Sona, G., Viviani, E., Bresci, E., & Preti, F. (2019). Multi-sensor UAV application for thermal analysis on a dry-stone terraced vineyard in rural tuscany landscape. *ISPRS International Journal of Geo-Information, 8*(87).
Vlotman, W. F., Smedema, L. K., & Rycroft, D. W. (2001). Modern land drainage. In *Planning, design and management of agricultural drainage systems*. CRC Press/Balkema.
Webb, N. P., Marshall, N. A., Stringer, L. C., Reed, M. S., Chappell, A., & Herrick, J. E. (2017). Land degradation and climate change: Building climate resilience in agriculture. *Frontiers in Ecology and the Environment, 15*(8), 450–459. https://doi.org/10.1002/fee.1530
Wemple, B. C., Swanson, F. J., & Jones, A. J. (2001). Forest roads and geomorphic process interactions, Cascade Range, Oregon. *Earth Surface Processes and Landforms, 26*, 191–204.
Westoby, M. J., Brasington, J., Glasser, N. F., Hambrey, M. J., & Reynolds, J. M. (2012). Structure-from-Motion' photogrammetry: A low-cost, effective tool for geoscience applications. *Geomorphology, 179*, 300–314.
Yamazaki, Y., Okazawa, H., Sekiyama, A., & Fujikawa, T. (2019). Accuracy verification of UAV-SfM survey of terrace paddy fields in a hilly and mountainous area. *IJERD – International Journal of Environmental and Rural Development, 10*(1), 153–159.
Yang, Z., Cai, H., Shao, W., Huang, D., Uchimura, T., Lei, X., Tian, H., & Qiao, J. (2019). Clarifying the hydrological mechanisms and thresholds for rainfall-induced landslide: In situ monitoring of big data to unsaturated slope stability analysis. *Bulletin of Engineering Geology and the Environment, 78*, 2139–2150. https://doi.org/10.1007/s10064-018-1295-5
Yu, W., Zhao, L., Fang, Q., & Hou, R. (2021). Contributions of runoff from paved farm roads to soil erosion in karst uplands under simulated rainfall conditions. *Catena, 196*.
Zhao, B., Dai, Q., Han, D., Dai, H., Mao, J., & Zhuo, L. (2019). Probabilistic thresholds for landslides warning by integrating soil moisture conditions with rainfall thresholds. *Journal of Hydrology, 574*, 276–287. https://doi.org/10.1016/j.jhydrol.2019.04.062